INVESTIGATION OF THE STRUCTURAL, OPTICAL AND ELECTRICAL PROPERTIES OF INDIUM-DOPED TiO_2 THIN FILMS GROWN BY PULSED LASER DEPOSITION TECHNIQUE ON LOW AND HIGH INDEX GaAs PLANES

Faisal S. Al mashary [a, b, *], Jorlandio F. Felix [c], Sukarno O. Ferreira [d], Daniele de Souza [e], Yara G. Gobato [e], Jasbinder Chauhan [a], Natalia Alexeeva [a], Mohamed Henini [a], Abdulrahman M. Albadri [f], Ahmed Y. Alyamani [f]

[a] School of Physics and Astronomy, University of Nottingham, Nottingham, NG7 2RD, United Kingdom
[b] Department of Physics, College of Science, Qassim University, Buraydah, 14452, Saudi Arabia
[c] Instituto de Física, Universidade de Brasília, Núcleo de Física Aplicada, 70910-900, Brasília, DF, Brazil
[d] Departamento de Física, Universidade Federal de Viçosa, 36570-900, Viçosa, MG, Brazil
[e] Departamento de Física, Universidade Federal de Sao Carlos, SP, Brazil
[f] National Center for Nanotechnology and Advanced Materials, King Abdulaziz City for Science and Technology, Riyadh, 11442, Saudi Arabia

* Corresponding author. School of Physics and Astronomy, University of Nottingham, Nottingham, NG7 2RD, United Kingdom
E-mail address: faisal.almashary@qu.edu.sa (F. S. Al mashary)

Abstract

The properties of In-doped TiO2 grown by Pulsed Laser Deposition on (100) and (311)B GaAs substrates have been investigated. X-ray diffraction and photoluminescence results have shown that samples grown on (311)B GaAs planes have better crystallographic properties than those grown on (100). Both anatase and rutile phases were detected in samples with lower In-doping (In=5

nm) while only rutile phase was observed for higher In-doped samples (In=15 nm). Furthermore, In-doping adversely affected the electrical properties of samples grown on (100) substrates while it enhanced those of (311)B samples. Two shallow defects were detected in all samples except for (311)B sample (In=15 nm) where three shallow defects were observed. The presence of more shallow defects in this sample is evidenced by a red-shift in the absorption spectrum. It was concluded that sample (311)B (In=15 nm) is best among all other samples and makes it more suitable for solar cell applications.

Keywords: In-doped TiO_2; Pulsed Laser Deposition; X-ray diffraction; Photoluminescence; Deep Level Transient Spectroscopy

1. Introduction

TiO_2 is a transparent conducting oxide (TCO) material which has been widely studied due to its remarkable properties, such as efficient photoactivity, high stability, low cost and non-toxicity [1-3]. It has been used in many applications such as photocatalysis [4], water and air purification [5], photo-electrochemical (PEC) water splitting [6], UV sensors [7-9] and as a solar cell [10, 11]. TiO_2 is a wide bandgap oxide semiconductor material which exists in nature in three polymorphs, namely anatase, rutile and brookite [12, 13]. Its wide bandgap (3.0-3.4 eV) [14, 15] makes it sensitive to UV light and not to visible light which limited its use as a solar cell. To overcome this limitation, surface modification, combination with other semiconductors, in addition to metal and non-metal ion doping have been used to make TiO_2 sensitive to the visible light [16]. Different metal ions such as Ag [17], Sb [18], Fe^{3+}, Mo^{5+}, Ru^{3+}, Os^{3+}, Re^{5+},

V^{4+}, Rh^{3+} [19] and In [20, 21] have been used as dopant in TiO_2 with the aim to increase the absorption of the visible light by modifying its electronic and optoelectronic properties. In the studies of indium doping of TiO_2 [20, 21], different growth techniques have been used to synthesise TiO_2 thin films on Si substrates.

GaAs is a direct bandgap semiconductor and one of the most studied III-V compound semiconductors [22]. The direct bandgap of GaAs makes it suitable for optoelectronics as compared to Si. Moreover, due to higher carrier mobility of GaAs as compared to Si, GaAs draws much attention for making high frequency devices [23, 24]. Furthermore, as GaAs has higher bandgap energy when compared to Si, that makes GaAs more suitable for devices that operate at high temperature. Additionally, the electrical, structural and optical properties of devices grown on high index planes of GaAs, i.e. (n11) where n is an integer, are improved when compared to the same devices grown on the conventional plane (100) [25]. For example, the morphological and optical properties of (InGa)As quantum dots (QDs) grown on (311)B GaAs substrates have been found to be superior to those grown on (100) GaAs substrates [26]. Additionally, the structural characteristics of InAs QDs grown on (311)B orientation are better than those grown on low index (100) plane [27]. All the above provide a great motivation to investigate the electrical and optical properties of In-doped TiO_2 grown on conventional and high index GaAs substrates rather than Si. Recently, TiO_2 has been employed as a gate oxide in GaAs metal-oxide-semiconductor field-effect transistor (MOSFET) due to its high dielectric constant [23, 28, 29]. In addition, TiO_2 was grown on GaAs substrates to study its photocatalytic applications [30]. The crystalline structure of TiO_2 grown by Pulsed Laser

Deposition (PLD) on semi-insulating (100) GaAs substrates was also investigated [31].To the best our knowledge, there is no single study of the electrically active defects in In-doped TiO_2 thin films grown by PLD technique on GaAs substrates. It is worth mentioning that previous studies on In-based and GaAs-based materials have shown that solar efficiency in these materials can be enhanced at the nanoscale range. In particular, an enhancement in electron-hole recombination has been observed in InP nanowires [32] and nanometer GaAs quantum well tube embedded inside AlGaAs/GaAs heterostructures [33]

Oxygen vacancies are well-known defects in TiO_2 which can alter the geometric structure and the chemical properties of the system [34]. Furthermore, incorporating indium into the TiO_2 host lattice could create defects within the forbidden bandgap of TiO_2. Understanding the deep and shallow level defects is essential for future devices [35]. Deep Level Transient Spectroscopy (DLTS) [36] is a powerful technique which can be used to investigate the electrically active defects. By DLTS, defects parameters, such as energy, capture cross section and concentration can be determined. Additionally, X-ray diffraction (XRD), current – voltage (I-V), capacitance – voltage (C-V) and photoluminescence (PL) measurements have been performed.

In this study, In-doped TiO_2 thin films have been grown on (100) and (311)B n-type GaAs substrates. The aim was to investigate the effect of the orientation of the GaAs substrates, i.e. (100) and (311)B, on the structural, optical and electrical (especially the electrically active defects) properties of In-doped TiO_2 thin films.

2. Sample Details

Two series of samples were prepared for this study using low and high index GaAs substrates, namely (100) and (311)B. For the first series, a layer of 380 nm TiO_2 thin film, measured using cross-section scanning electron microscopy (SEM, HITACHI S4500), was deposited on (100) n-type GaAs substrate using pulsed laser deposition (PLD/MBE 2100) from PVD products. The laser source was a KrF excimer Laser (λ = 248 nm, pulse width 20 ns, and repetition rate = 10 Hz) operating at 350 mJ to ablate the target with two sets of pressures (under vacuum: 10^{-6} Torr and with oxygen background pressure: 5×10^{-3} Torr). The growth temperature was fixed at 500 ˚C and the distance from the substrate to target was set at 55 mm. All parameters which contribute to the growth rate were kept constant during the operating time. This series of samples is named (100) samples. By thermal evaporation, two layers of indium (15 and 5 nm thick) were deposited on top of two 380 nm TiO_2 thin films grown on (100) GaAs substrates. In order to incorporate indium into the TiO_2 lattice, samples were annealed under oxygen flow with a temperature ramp rate of 15°C/minute and a dwelling temperature of 500 °C for 30 minutes. This annealing process has been found as the best among many annealing processes and procedures (not shown here). Therefore, this series consists of two samples, namely 15 nm and 5 nm In doped TiO_2/ n-type (100) GaAs, which were labelled as 15 (100) and 5 (100), respectively.

For the second series, it is exactly the same as the first series except that the GaAs substrate orientation is (311)B. These were labelled as 15 (311)B and 5 (311)B.

A third series of TiO_2 thin film control samples, which do not contain In, were grown by PLD technique on both GaAs planes using the same procedures as

described above. These are referred to as (100) and (311)B samples. This will allow us to investigate the effect of In doping.

To prepare the samples for electrical characterization, a shadow mask with circular mesas was used to deposit Au on top of the In-doped TiO_2 layer to create Schottky contacts. In the back side of the GaAs substrates, Ge/Au/Ni/Au were deposited and then annealed at 390 ^{0}C for 20 minutes to create back Ohmic contacts. It is worth to mention that the back contacts were deposited on the back of the substrates before the growth of TiO_2 thin films.

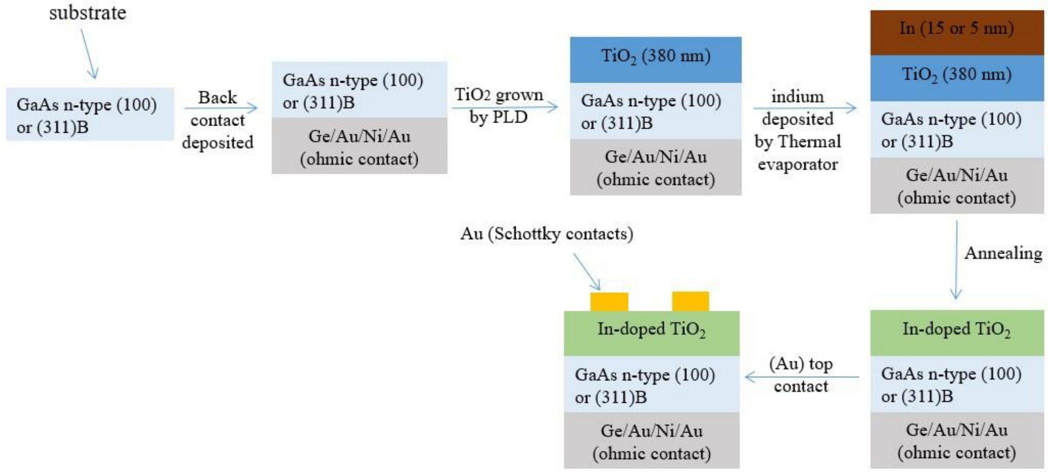

Fig. 1 shows the growth and fabrication steps.

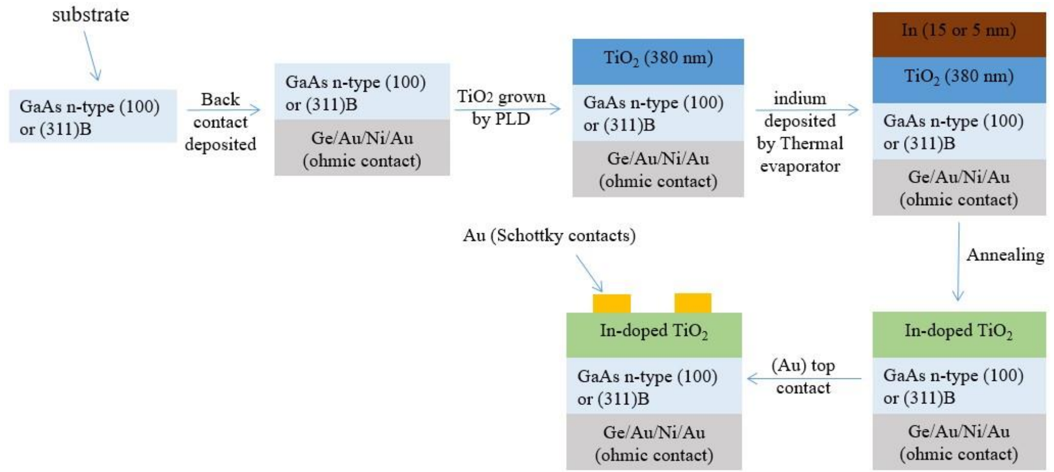

Fig. 1 Growth and metallisation steps.

The XRD measurements were performed using a Bruker D8 Discover Diffractometer equipped with the Cu K_α radiation (1.5418 Å). The Glancing Angle X-ray Diffraction method was used with grazing incidence angle of 2°. The optical absorption measurements were performed on the samples using a UV–Visible spectrophotometer (UV-2700, Shimadzu, Tokyo, Japan). The optical properties of In doped TiO_2 thin films were investigated using PL as a function of temperature using a laser excitation wavelength of 325 nm from a He-Cd laser. I-V characteristics were obtained using a Keithley 236 source measure unit. C-V characteristics were investigated at 300 K with 1 MHz frequency using Boonton 7200 capacitance meter. DLTS measurements were carried out using a He closed-loop cycle cryostat (Janis CCS-450) and Boonton 7200 capacitance meter.

3. Results and Discussion

3.1. Structural Measurements

The x-ray diffraction spectra of all doped samples are shown in Fig. 2. As illustrated in Fig. 2 (a) and (b), both anatase and rutile phases of TiO_2 are present

in sample 5 (100) and 5 (311)B , but the rutile phase is dominant. However, for samples 15 (100) and 15 (311)B, only a single-phase rutile was obtained as revealed in Fig. 2 (c) and (d), respectively. Moreover, the crystallographic properties of the samples in series (311)B, i.e. 5 (311)B and 15 (311)B, are clearly better than the samples in series (100). The peaks shown in Fig. 2 are in good agreement with the standard spectrum (JCPDS no.: 84-1286 and No: JCPDS 88-1175) for anatase and rutile phases, respectively. Finally, XRD results show that the thickness of the indium film has a remarkable influence on the structural properties of the TiO_2 thin films, as both anatase and rutile phases can be observed for the low doped samples, whereas only one phase, i.e. rutile, could be detected for both highly doped samples.

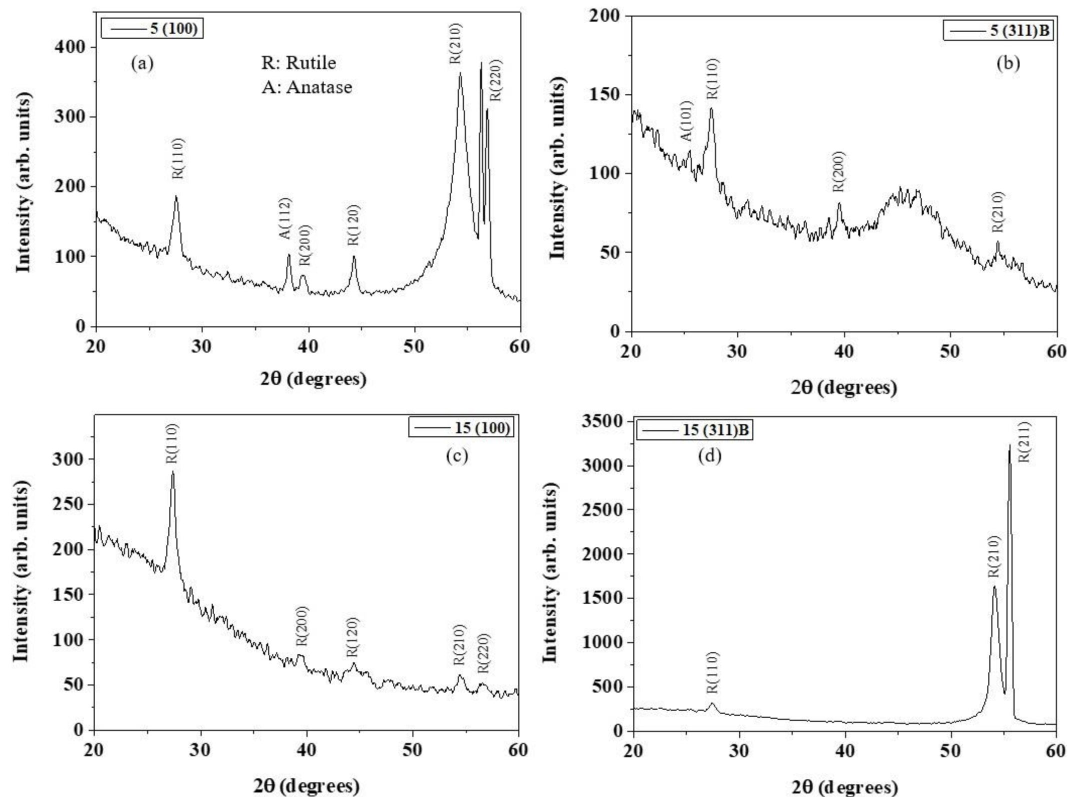

Fig. 2: X-ray diffraction pattern of sample (a) 5 (100), (b) 5 (311)B, (c) 15 (100) and (d) 15 (311)B.

Fig. 3 shows the absorption spectra measured at room temperature for all doped samples. As Fig. 3 depicts, an absorption band centred at 3.65 eV is observed in sample 5 (311)B and at 3.30 eV in sample 15 (311)B. This redshift in the absorption is an indication that the increase in the thickness of the indium film enhances the doping concentration of the TiO_2 thin films. However, for samples in (100) series, a small absorption band that is centred at approximately 3.65 eV is observed for sample 5 (100) and no relevant change was observed in the absorption spectra with increasing indium, i.e. sample 15 (100). From the results of Fig. 3, the absorption coefficient (α) above the threshold of fundamental absorption has been calculated using the $(E-E_g)^2$ energy dependence characteristic for indirect allowed transitions to obtain $(\alpha h\nu)^{1/2}$ versus photon energy (E) plot (h is Planck's constant and ν is the frequency). Fig. 4 shows the $(\alpha h\nu)^{1/2}$ versus photon energy (E) plot and the values of optical absorption gaps obtained by extrapolation are 3.39, 3.34, 3.40 and 2.94 eV for sample 5 (100), 5 (311)B, 15 (100) and 15 nm (311)B, respectively. It is clear that due to the increase of indium content in series (311)B samples, the bandgap has been reduced from 3.34 eV for sample 5 (311)B to 2.94 eV for sample 15 (311)B (see Fig. 4). However, no significant change has been noticed in series (100). Therefore, the indium doping process of TiO_2 thin films has a remarkable influence on the bandgap of the samples grown on (311)B GaAs substrates.

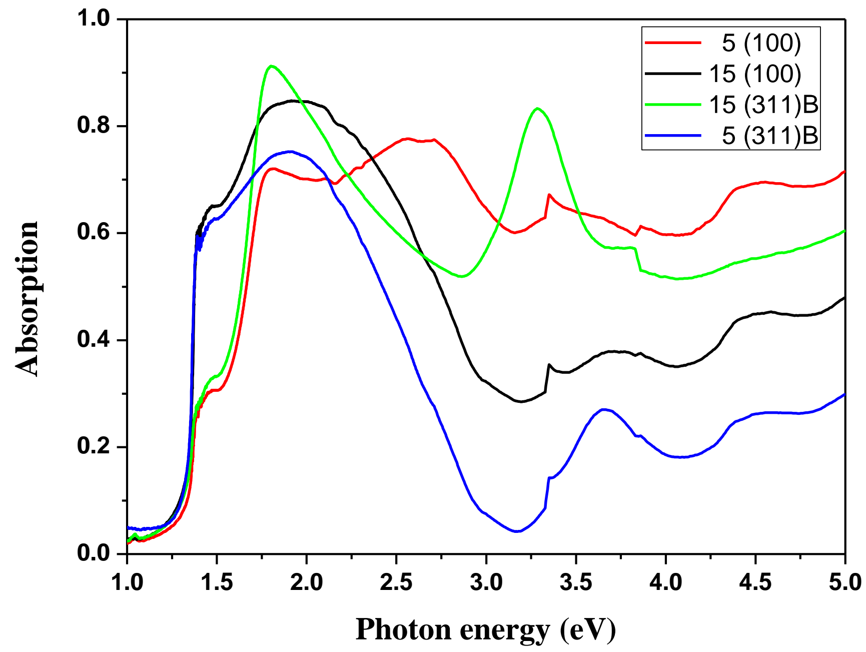

Fig. 3: Optical absorption spectra at room temperature for all In-doped samples.

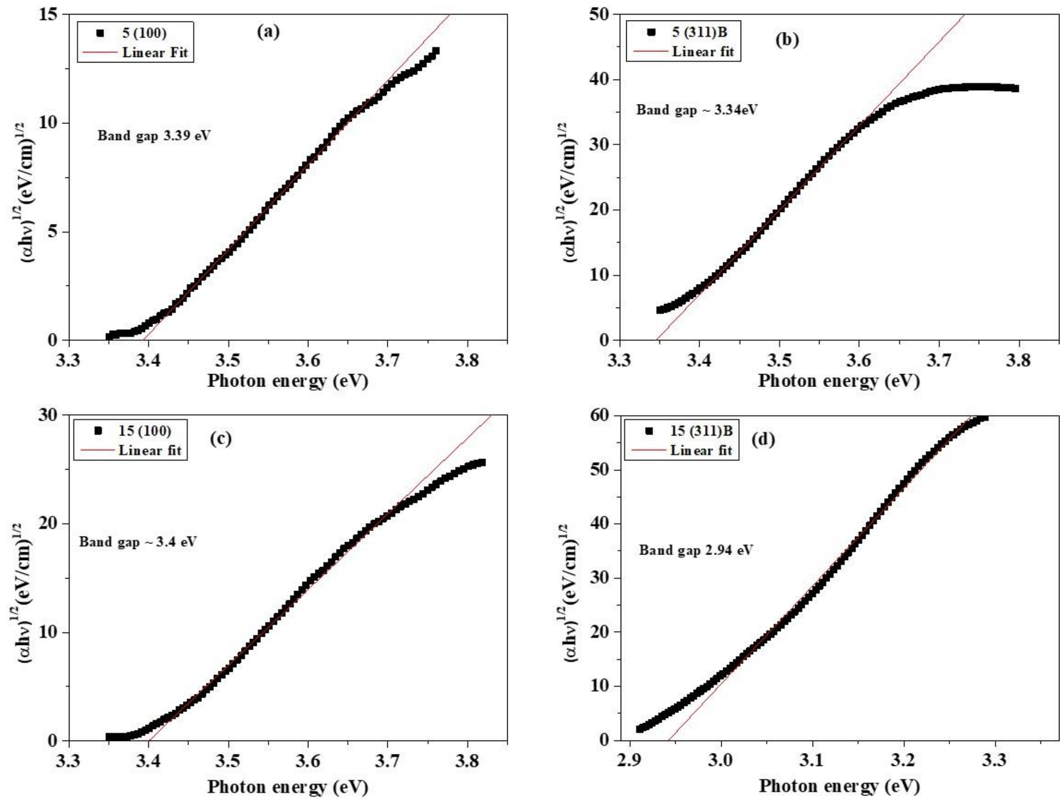

Fig. 4: $(\alpha h\nu)^{1/2}$ versus photon energy (E) plots for samples (a) 5 (100), (b) 5 (311)B, (c) 15 (100) and (d) 15(311)B samples.

3.2. Current-Voltage Characteristics

The semi-logarithmic plot of current density (J) versus applied bias (J-V) measurements at room temperature for all samples are shown in Fig. . As can be seen in this figure for the doped samples, samples grown on (100) GaAs have higher reverse current density as compared to (311)B GaAs samples. In particular, sample 15 (311)B has the lowest reverse current and sample 15 (100) has the highest reverse current. However, for the control samples (undoped), sample (100) has the lowest reverse current and samples (311)B has the highest reverse current when compared to all other samples. Current density-voltage (J-V) measurements as function of temperature have been carried out for all samples in the range of 20-300 K (with 20 K intervals) to extract the diode parameters.

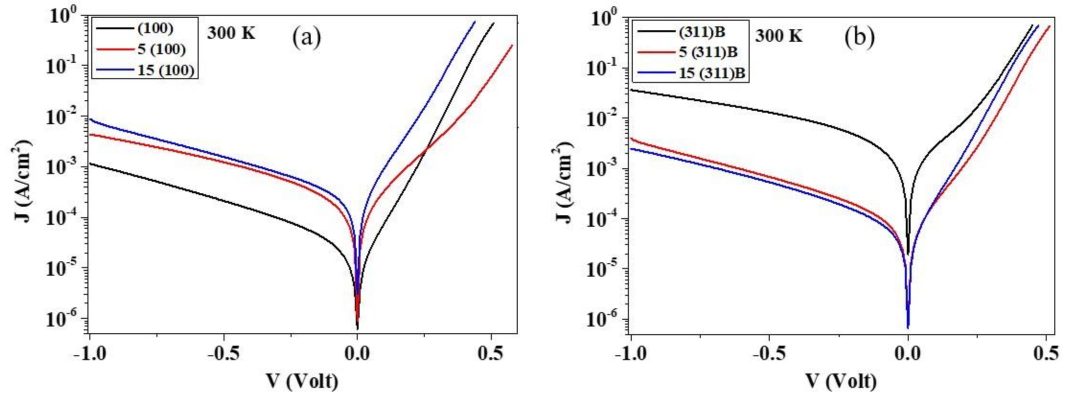

Fig. 5: Semi-logarithmic J-V plots for (a) series (100) samples and (b) series (311)B samples.

The thermionic emission model describes the I-V characteristics, including series resistance (R_s), of an ideal diode as follows [37]:

$$I = I_0[exp\left(\frac{q(V-IRs)}{nKT}\right) - 1] \tag{1}$$

where $I_0$is the saturation current and is given by:

$$I_0 = AA^*T^2\, exp\left(\frac{-q\phi_b}{KT}\right) \tag{2}$$

In Equations (1) and (2), q is the elementary charge, n is the ideality factor, k is Boltzmann's constant, T is the temperature, ϕ_b is the barrier height, R_s is the series resistance, A is the effective diode area (A = 3.85 x 10^{-3} cm^2 for sample 5 (100) and A = 1.26 x 10^{-3} cm^2 for the other samples) and $A^*$is the effective Richardson's constant (A^* = 671 $A.cm^{-2}.K^{-2}$ for TiO_2 [38]). Werner's method was used to calculate the diode parameters (n, ϕ_b and R_s) [39]. These parameters for all samples at room temperature are summarised in Table 1. As Table 1 shows, for samples grown on GaAs (100) substrates, the (100) control sample has the lowest ideality factor (1.56) and highest barrier height (0.79 eV) values as compared to all samples [(100) and (311)B] investigated here. Sample 15 (100) has lower ideality factor and barrier height as compared to sample 5 (100) whereas the series resistance is lower for sample 5 (100). Therefore, indium doping has adversely affected the electrical properties of TiO_2 thin films grown on (100) GaAs substrates. However, for samples grown on GaAs (311)B substrates, as the concentration of indium decreases, the barrier height increases and the ideality factor decreases. In particular, for sample 5 (311)B, the barrier height and ideality factor are 0.77 eV and 1.64, respectively. However, for sample 15 (311)B, the barrier height and ideality factor are 0.74 eV and 1.74, respectively. It is worth mentioning that the (311)B control sample has the lowest barrier height (0.70 eV) and the highest ideality factor (1.87) when compared to the doped samples in series (311)B. Thus, the electrical properties of TiO_2 thin films grown on (311)B GaAs substrates have been enhanced by indium doping. Among all doped samples, sample 5 (311)B has the highest barrier height and the lowest ideality factor which may indicate that this sample has the best electrical properties of as compared to all other doped samples.

Table 1: Ideality factor (n), barrier height (ϕ_b) and series resistance (R_S) at room temperature for samples 15 (100), 5 (100), 15 (311) and 5 (311)B.

Sample	n	ϕ_b (eV)	R_S (kΩ)
(100)	1.56	0.79	22.19
5 (100)	2.01	0.76	1.46
15 (100)	1.71	0.72	12.58
(311)B	1.87	0.70	1.43
5 (311)B	1.64	0.77	20.22
15 (311)B	1.74	0.74	15.73

The plot of ln (I_0/T^2) versus 1000/T follows a straight line for samples (100), 15 (100), 5 (100), (311)B, 15 (311)B and 5 (311)B in a temperature range of 220-300 K, 180-300 K, 220-300 K, 180-300 K, 240-300 K and 200-300 K, respectively (Fig. S1 in the supplement). The straight line behaviour indicates that the conduction mechanism could be governed by thermionic emission and the saturation current (I_0) can be obtained from Equation (2) [40]. However, at low temperatures a deviation from linearity is noticed for each sample and that could be due to a contribution of additional current as a result of the reduction in the barrier height [25].The experimental Richardson's constant, calculated from the y-intercept of the straight line, was found to be 6.4 x 10^{-7}, 2.5 x 10^{-4}, 3.0 x 10^{-4}, 3.6 x 10^{-6}, 7.4 x 10^{-4} and 1.8 x 10^{-7}A cm^{-2} K^{-2} for samples (100), 15 (100), 5 (100), (311)B, 15 (311)B and 5 (311)B, respectively. The Richardson's constants that are obtained for all samples are much lower than the well-established value

$A^* = 671$ A cm^{-2} K^{-2} for TiO_2. This deviation could be due to the spatial inhomogeneous barrier heights and potential fluctuations at the interface [41]. This behaviour has also been observed in a previous study of In-doped TiO_2 grown by PLD on Si substrates [21].

The variation of barrier height and ideality factor with temperature (Fig. S2 in the supplement) is usually observed in many metal-semiconductors interfaces [42]. The barrier height increases with increasing temperature while the ideality factor decreases as temperature increases for all samples. This behaviour is well-known and is due to nonuniformity of interfacial charges and barrier inhomogeneity [21, 43, 44]. At low temperature, carriers are frozen and therefore the current passes through the interface states which results in higher values of the ideality factor [45]. Note that the carriers, at low temperature, can surmount the lower barriers and the mechanism of transport will be dominated by the current flowing through the region with lower barrier heights. As temperature increases, more carriers will gain sufficient energy to surmount the higher barriers, which results in an increase of the barrier height calculated at high temperatures [46].

The plots of the reverse current versus inverse temperature could be used to calculate the main traps which contribute to the leakage current [45]. The plots of reverse current versus 1000/T at -1 V voltage bias (Fig. S3 in the supplement) show that only one trap was detected for each sample and its activation energy was found to be 0.11 ± 0.01, 0.09 ± 0.01, 0.14 ± 0.01 and 0.15 ± 0.01 eV for 15 (100), 5 (100), 15 (311)B and 5 (311)B samples, respectively. As seen above, a similar trap is observed in each series of (100) and (311)B but the activation energy is higher in series (311)B. T. Miyagi, *et al.* in their study of photocatalytic property and deep levels of Nb-doped anatase TiO_2 films grown by metal organic

chemical vapor deposition have assigned a defect with energy of 0.13 eV in undoped TiO_2 to oxygen vacancies or interstitial Ti ion [47]. Therefore, the origin of the defect that has been detected in 15 (311)B and 5 (311)B samples could also originate from oxygen vacancies or interstitial Ti ion.

3.3. Capacitance-Voltage Characteristics

The capacitance-voltage (C-V) measurements at room temperature, **Error! Reference source not found.**6, have been carried out for all doped samples in order to calculate the free carrier concentrations. As **Error! Reference source not found.**6 shows, sample 5 (100) has the highest capacitance, as it has the highest area when compared with all other samples, while sample 15 (311)B has the lowest capacitance. The free carrier concentrations, N_d, for all doped samples were calculated using the slope of the best fit of the plot $1/C^2$ versus reverse bias, as shown in Fig. 7. The doping concentration is found to be uniform for all doped samples as proven by the linear behaviour of the plot of $1/C^2$ versus applied bias. The free carrier concentration is about 3.44×10^{17} cm^{-3}, 3.63×10^{17} cm^{-3}, 4.98×10^{17} cm^{-3} and 6.41×10^{17} cm^{-3} for samples 15 (100), 5 (100), 15 (311)B and 5 (311)B, respectively. Moreover, Fig. 8 shows the C-V and the plot of $1/C^2$ versus reverse bias for the control samples, i.e. sample (100) and (311)B. The doping concentration in the control samples is also uniform and the free carrier concentration is found to be 1.14×10^{18} cm^{-3} and 2.96×10^{17} cm^{-3} for sample (100) and (311)B, respectively.

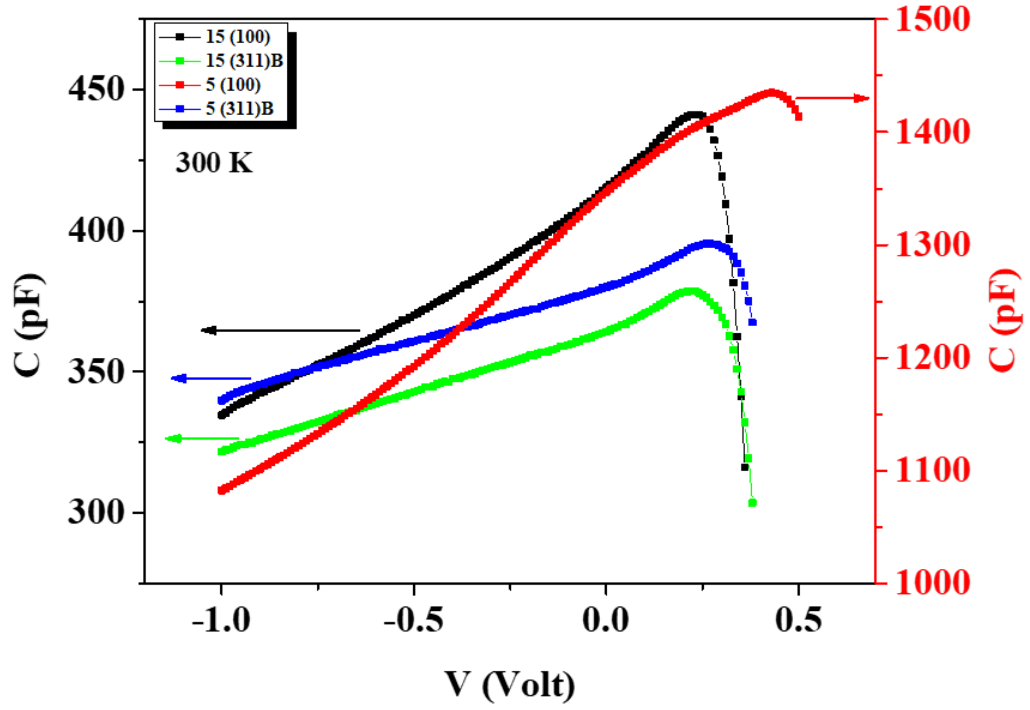

Fig. 6: C-V plot at room temperature for all doped samples.

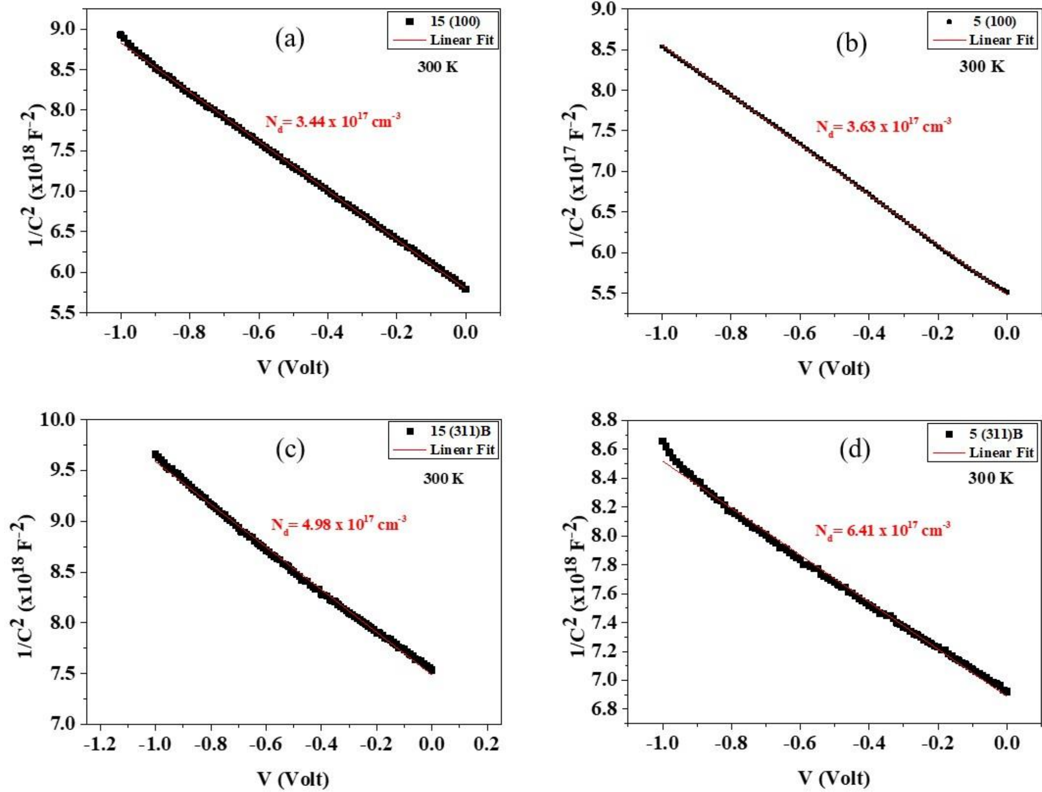

Fig. 7: $1/C^2$ versus applied bias plots at room temperature for (a) 15 (100), (b) 5 (100), (c) 15 (311)B and (d) 5 (311)B samples.

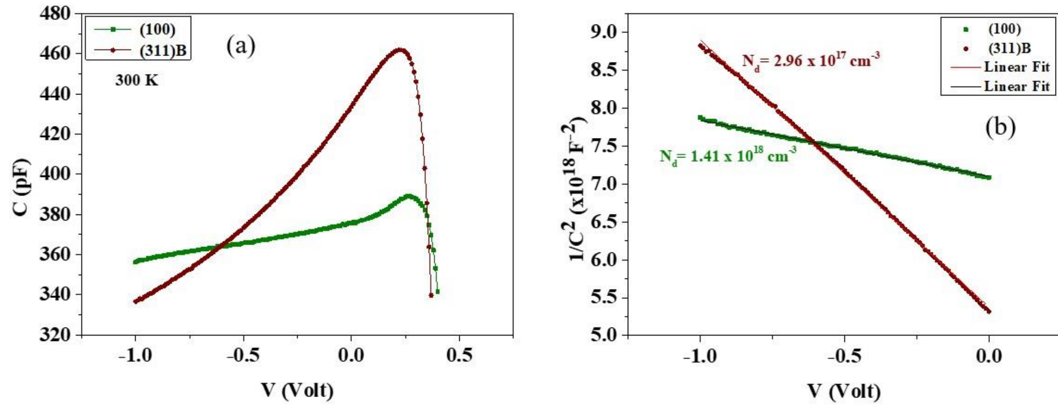

Fig. 8: (a) C-V and (b) $1/C^2$ versus applied bias plots at room temperature for control samples.

3.4. Photoluminescence Measurements

Fig. 9 (a) and (b) show typical PL spectra at different temperatures for sample 5 (100) and 5 (311)B, respectively. For both samples, the PL spectra clearly shows a visible broad band around 2.2 eV. A broad absorption band around 2.1 eV was also observed in Fig. 3. This emission is usually associated with the presence of anatase phase of TiO_2 thin films [21, 48, 49]. Moreover, it was found that both samples, i.e. 5 (100) and 5(311)B, also exhibit a broad near infra-red (NIR) band at 300 K around 1.5 eV, which could be associated with an emission due to the rutile phase [48, 49]. An absorption band around 1.5 eV is also clearly seen in Fig. 3. Actually, several previous works have reported that the anatase phase of TiO_2 usually exhibits PL bands around 1.9 eV (red emission) and 2.4 eV (green emission) while the rutile phase usually exhibits PL bands around 1.5 and 1.7 eV [48]. The green emission associated with the anatase phase is usually attributed to self-trapped excitons [50], oxygen vacancies [51] or to a radiative recombination of free electrons with trapped holes. These trapped holes

could be localized at oxygen vacancies sites (V_O) or at Ti sites adjacent to V_O [48]. On the other hand, the red PL emission observed for the anatase phase is usually assigned to the optical recombination between trapped electrons and free holes [48]. Particularly, it was also previously shown that the rutile phase samples are less sensitive to prolonged exposure to UV illumination in oxygen environment than anatase samples. This fact could support the possible interpretation that the NIR PL could be associated with a possible radiative recombination between midgap trapped electrons and free holes at the valence band [48]. However, the nature of NIR emission associated with the rutile phase and the visible emission associated with the anatase phase in TiO_2 are not well understood. In general, our PL results for both 5 (100) and 5 (311)B samples, which are fully consistent with the presence of mixed anatase and rutile phases, are in good agreement with XRD and absorption results.

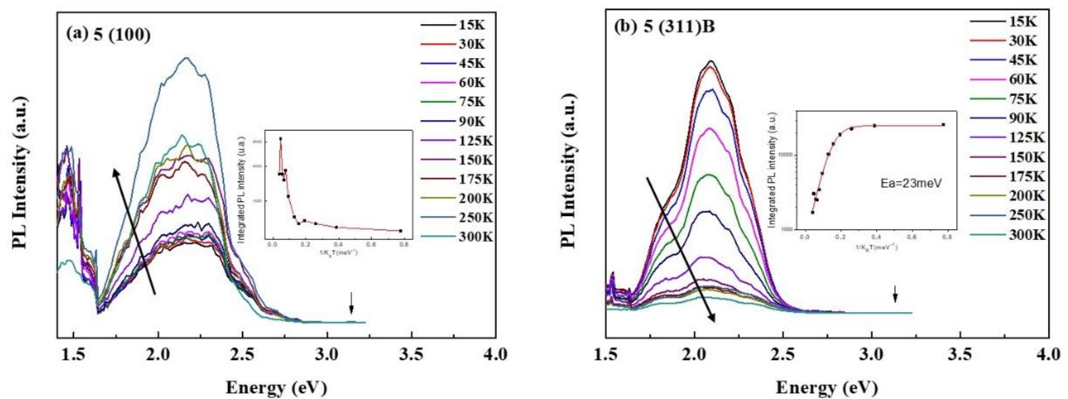

Fig. 9: Temperature dependence of PL spectra for sample (a) 5 (100) and (b) 5 (311)B. The arrows show the increasing of temperature. The inset shows the Arrhenius plots.

The PL spectra of sample 15 (100) and 15 (311)B are shown in Fig. 10. For both samples, emissions in visible and infrared regions have also been

observed. This observation is fully consistent with the presence of anatase and rutile phases, as observed in the low doped samples, which indicates a mixed phase for these samples. However, only rutile phase was detected using XRD technique in both 15 (100) and 15 (311)B. A possible explanation is that the PL technique is more sensitive for probing structural phases of thin films than XRD technique. Therefore, although not be detected by XRD, the anatase phase is present in both samples. Another possible explanation is that the visible emission in both samples is not due to the presence of anatase phase but could be related to a possible formation of In_2O_3 phase or doping effects [20, 21, 52].

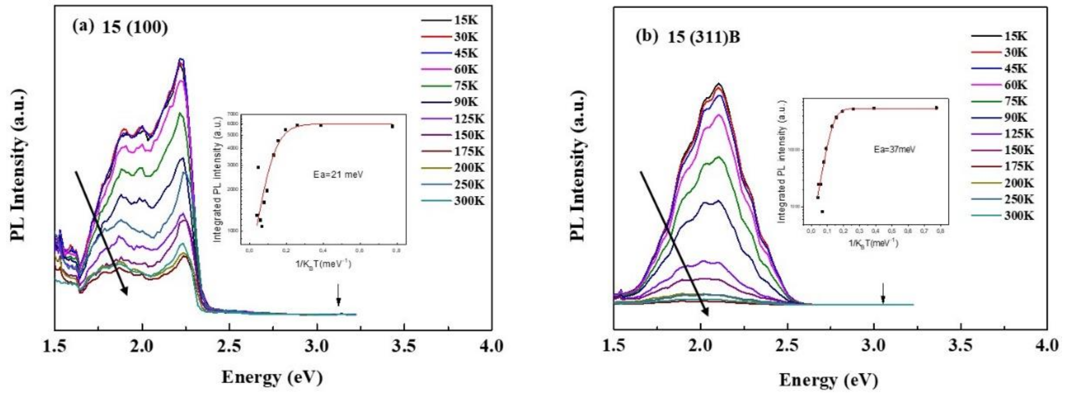

Fig. 10: Temperature dependence of PL spectra for sample (a) 15 (100) and (b) 15 (311)B. The arrows show the increasing of temperature. The inset shows the Arrhenius plots.

Furthermore, It was also observed that the PL bands are more intense in (311)B samples as compared with (100) samples (not shown here). These results seems to be consistent with the crystallographic properties of the samples in series (311)B that are clearly better than the samples in series (100).

In addition, for all doped samples at low temperatures, sharp peaks were also observed around 1.5 eV and were associated with typical emissions from the GaAs substrates as expected [53]. Moreover, all doped samples have also shown a

small peak around 3.14 eV which could be associated with a small contribution of the brookite bandgap of TiO_2 or In doping effects[54].

The temperature dependence of the emission bands shows that the emission intensity of the PL peaks increases considerably with the decrease of temperature as expected. The activation energy have been estimated using the standard Arrhenius equation [55]:

$$I(T) = \frac{I_0}{1+\gamma \exp\left(-E_a/(k_B T)\right)} \quad (3)$$

where $k_B$is the Boltzmann constant, I_0 is the PL integrated intensity at 0 K, γ is the ratio between radiative and non-radiative lifetimes and E_a is an activation energy.

The Arrhenius plots are shown in the inset of Fig. 9 and 10. An activation energy of around 23 meV and 37 meV have been observed for sample 5 (311)B and 15 (311)B, respectively. Therefore, an increase of the activation energy was observed with the increase of indium content. Similar behaviour was observed previously by N. Al Saqri, *et al.* in their study of In-doped TiO_2 grown by e-beam evaporation on Si substrates [20]. However, for the sample 5 (100), an anomalous behaviour was observed for the temperature dependence of PL spectrum. It was observed that the PL intensity increases as the temperature increases up to 250 K and then decreases with increasing temperature in the range of 250 to 300 K as expected. This behaviour could be associated with a possible charge transfer or traps due to the presence of defects or some disorder in TiO_2 which could localize the carriers non-radiatively. As the temperature increases, the trapped carriers can be thermally activated and could contribute to the optically active states which lead to an increase of the intensity of the PL with increasing temperature up to

250 K [56]. In contrast, for sample 15 (100), a standard behaviour was observed and an activation energy of about 21 meV was obtained.

Finally, it is worth mentioning that a possible formation of In_2O_3 after the thermal annealing treatment, especially for samples with high indium content, could also contribute to the observed PL bands. Thus, all these observed emission bands were attributed to the localized levels in the bandgap and could be due to intrinsic defects in TiO_2 and/or In_2O_3 as both usually have emissions in the same energy ranges. A possible contribution of In_2O_3 is particularly important for the In (15 nm)-doped TiO_2 samples. Therefore, it is difficult by using only PL measurements to separate between the contributions of defect-related emissions in TiO_2 and In_2O_3.

3.5. DLTS and Laplace DLTS Measurements

DLTS measurements have been performed for all samples, as Fig. 11 shows, over the scanned temperature range of 10 -300 K with a reverse bias V_R= -1V, filling pulse height V_P = 0V, filling pulse time t_P = 1 msec and rate windows of 200 s^{-1}. A very broad peak has been detected in each sample as shown in Fig. 11. Laplace DLTS [57], which is a powerful technique for resolving the broader peaks, has been used. Laplace DLTS measurements have revealed two traps in samples 15 (100), 5 (100) and 5 (311)B whereas three traps have been observed in sample 15 (311)B. It is worth mentioning that all these traps are shallow traps. Fig. 12 illustrates the Arrhenius plots for the traps in each sample which have been determined from Laplace DLTS measurements. The parameters of all traps in each sample are summarised in Table 2.

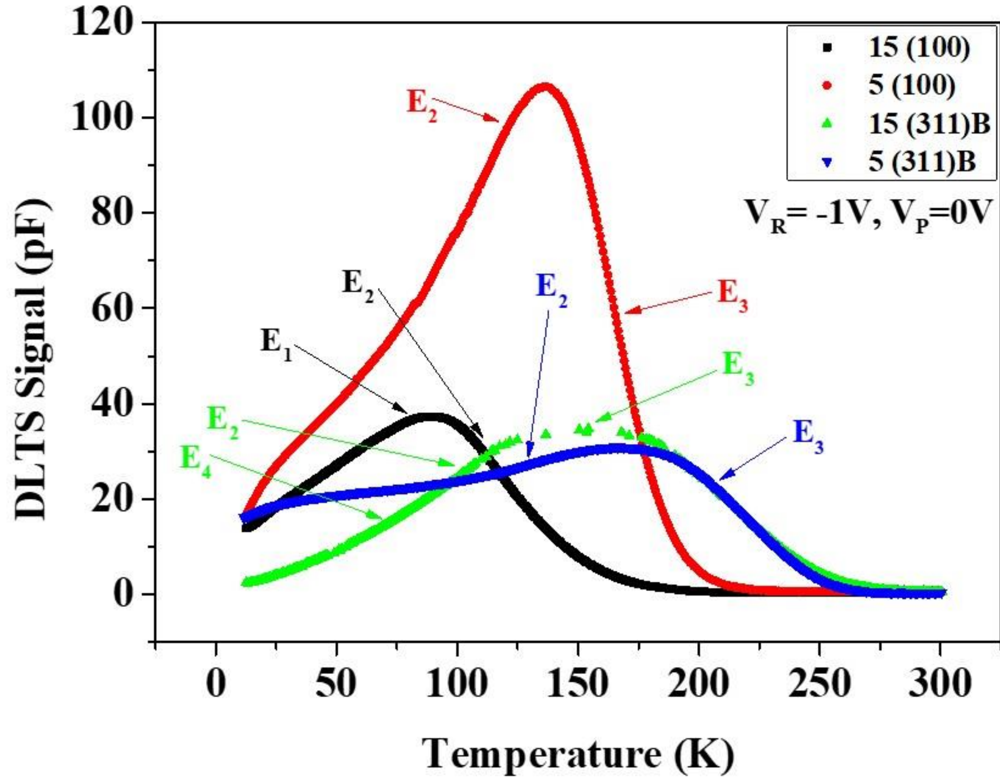

Fig. 11: DLTS signal for 15 (100), 5 (100), 15 (311)B and 5 (311)B samples.

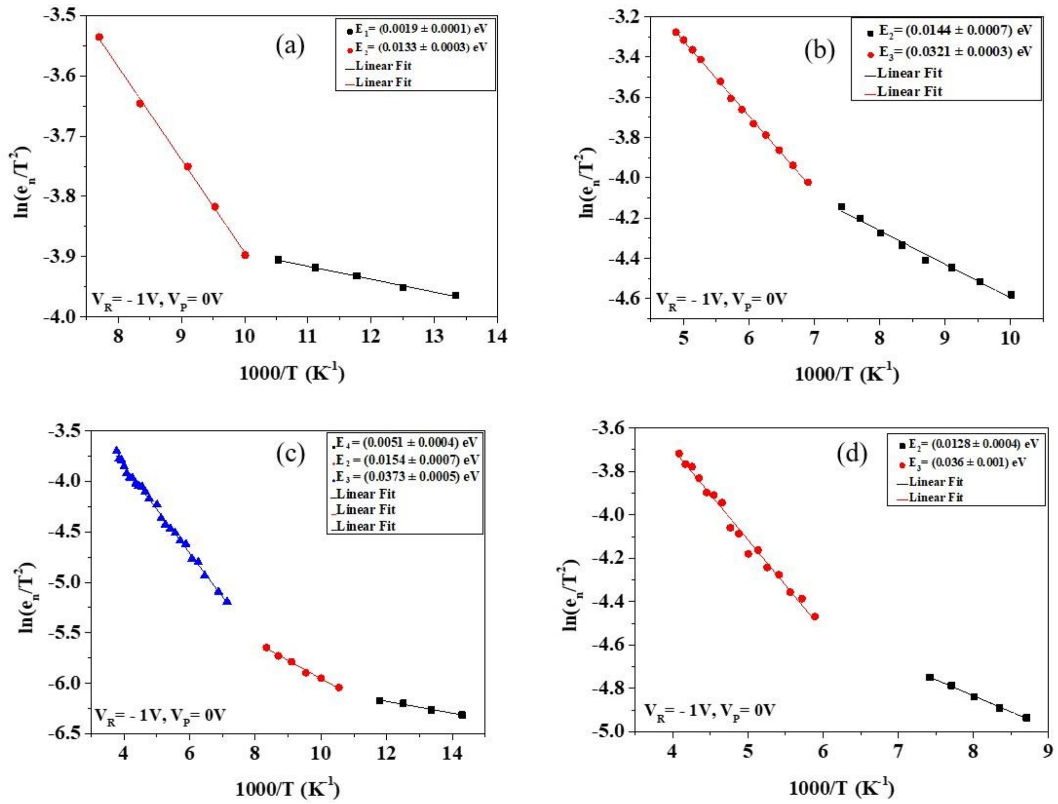

Fig. 12: Arrhenius plots from Laplace DLTS with reverse biases, V_R= -1 V, filling pulse height, V_P = 0V, and filling pulse time, t_P = 1 msec, for sample (a) 15 (100), (b) 5 (100), (c) 15 (311)B and (d) 5 (311)B.

Table 2: Traps parameters for 15 (100), 5 (100), 15 (311)B and 5 (311)B samples at V_R= -1V, V_P= 0V and t_P= 1 msec.

Sample	Trap	Activation Energy (eV)	Capture Cross-Section (σ_∞) (cm^2)	Trap Concentration (cm^{-3})
15 (100)	E_1	0.0019 ± 0.0001	8.17x 10^{-23}	4.50 x 10^{16}
	E_2	0.0133 ± 0.0003	3.08x 10^{-22}	2.31 x 10^{16}
5 (100)	E_2	0.0144 ± 0.0007	1.73 x 10^{-22}	6.05 x 10^{16}
	E_3	0.0321 ± 0.0003	7.55x 10^{-22}	3.36 x 10^{15}
15 (311)B	E_4	0.0051 ± 0.0004	1.36x 10^{-23}	3.85 x 10^{16}
	E_2	0.0154 ± 0.0007	5.04x 10^{-23}	4.60 x 10^{16}
	E_3	0.0373 ± 0.0005	3.92x 10^{-22}	8.04 x 10^{16}
5 (311)B	E_2	0.0128 ± 0.0004	8.43x 10^{-23}	8.17 x 10^{16}
	E_3	0.036 ± 0.001	4.31x 10^{-22}	6.65 x 10^{16}

As shown in Table 2, trap E_2 is present in each sample but with higher concentration, ~ 8.17 x 10^{16}, in sample 5 (311)B, while trap E_3 is detected in each samples except sample 15 (100). Trap E_3 has the highest concentration (~ 8.04 x $10^{16}cm^{-3}$) in sample 15 (311)B . Trap E_1 is found only in sample 15 (100) and trap E_4 has been detected only in sample15 (311)B. Trap E_1 was detected for the first time in our previous study of In-doped TiO_2 grown on Si substrate [21]. The origin of this trap is still unknown. To the best of our knowledge, the other defects, i.e. E_2, E_3 and E_4, are new and observed here for the first time. A theoretical model is needed to understand the origin of these defects.

DLTS measurements have been also carried out on control samples, (100) and (311)B, in order to investigate the effect of In incorporation on the traps. In other words, to investigate if the traps, E_1, E_2, E_3 and E_4, are present in the control samples or not. Fig. 3 (a) and (b) show the DLTS measurements whereas the Arrhenius plots, which were obtained from Laplace DLTS measurements, are

depicted in Fig. (c) and (d) for the control samples. In sample (100), two traps were detected, namely E_2 = 0.017 ± 0.001 and E_3 = 0.038 ± 0.001 eV. Incorporating 5 nm of indium into sample 5 (100) has not introduced any additional trap as the traps E_2 and E_3 in sample 5 (100) were also detected in the control sample (100). However, as indium doping increases, 15 nm, trap E_2 still could be detected but trap E_3 has been annihilated in sample 15 (100). In addition, trap E_1 in sample 15 (100) could not be detected in the control sample (100) nor in sample 5 (100), and hence it could be attributed to the larger indium incorporation which may form some complexes. For sample (311)B, a broad peak has been resolved by Laplace DLTS and two traps were detected, namely E_4= 0.0068 ± 0.0003 and E_3 = 0.034 ± 0.004 eV. In sample 5 (311)B, trap E_4 is removed and a new trap, E_2, was created as compared with the control sample (311)B. However, as indium doping increases, 15 nm, the same traps detected in the control sample are still observed in sample 15 (311)B, i.e. E_4 and E_3, in addition to the new trap E_2. Therefore, for the samples grown on (311)B plane, the creation of trap E_2 could be due to incorporating indium into TiO_2 lattice.

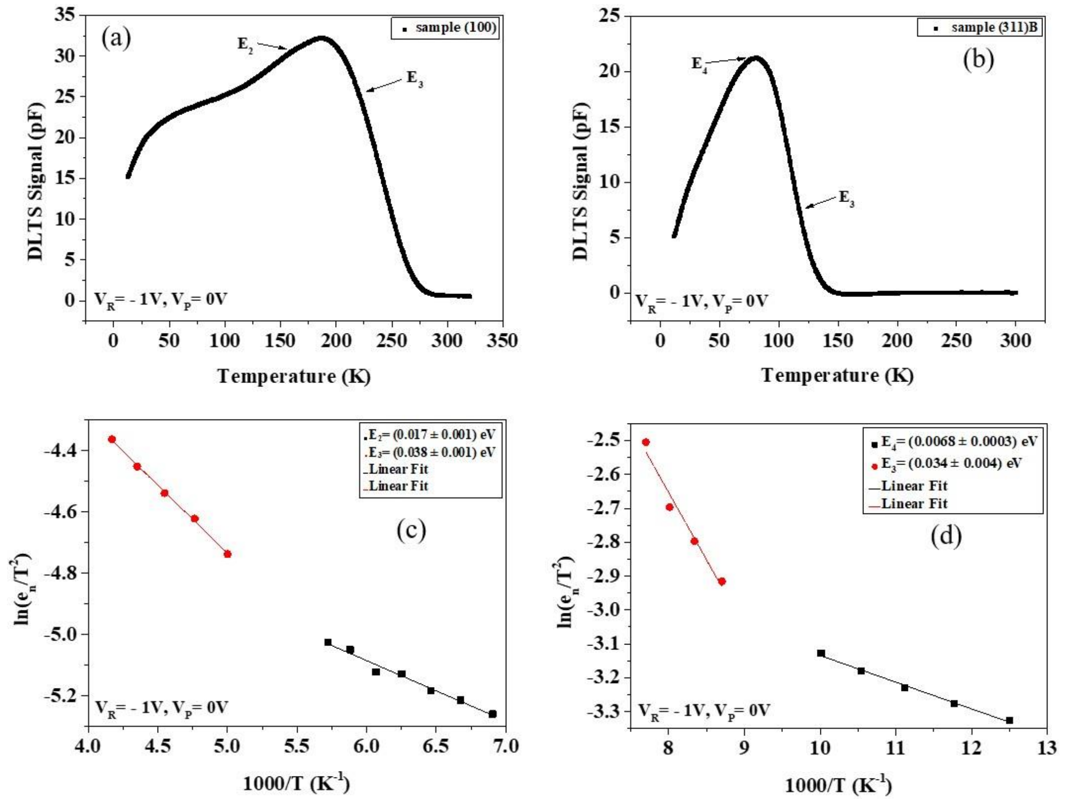

Fig. 13: DLTS signals for control samples (a) (100) and (b) (311)B. Arrhenius plots from Laplace DLTS measurements for (c) (100) and (d) (311)B control samples.

It is worth mentioning that the defects detected from I-V measurements could not be identified using DLTS techniques and that could be due to small concentrations of these defects. The broad DLTS peaks and the small concentrations of the defects detected from I-V measurements could be the reason of not observing such defects even when Laplace DLTS has been employed.

The formation of more shallow defects in sample 15 (311)B could be correlated with the reduction of its optical absorption gap (2.94 eV) as compared to the other doped samples. This low emission energy observed only in sample 15 (311)B could be accounted for by the presence of more shallow defects that form

a band of states under the conduction band, i.e. emission from valence band to donor states.

4. Conclusion

In this study, In-doped TiO_2 thin films were grown by PLD technique on low, (100), and high, (311)B, index GaAs planes. Two contents of indium, 5 and 15 nm, have been used. The I-V measurements at different temperatures were performed for all samples. At room temperature, sample 5 (311)B exhibits the lowest ideality factor, 1.64, and highest barrier height, 0.77 eV as compared to the other doped samples. DLTS technique has been used to investigate the electrically active defects in all samples. Two shallow traps have been detected in all samples except sample 15 (311)B where three shallow traps have been observed. To the best of our knowledge, all these shallow traps are reported here for the first time except for trap E_1. The XRD and PL measurements have shown that the samples grown on (311)B planes have better crystallographic properties when compared with samples grown on the conventional plane (100). In addition, both anatase and rutile phases were detected in lower In doped samples. On the other hand, only rutile phase was observed in higher In doped samples. The PL spectra have shown visible and near infrared bands in lower In doped samples as expected for the mixed rutile and anatase phases. The temperature dependence of the emission bands showed an increase of the activation energy with increasing In doping for (311)B samples. An absorption at lower energy (less than the expected bandgap energy) has been observed in sample 15 (311)B and this was attributed with the presence of more shallow donor defects as compared with the other samples. The formation of more shallow defects in sample 15 (311)B that led to a red-shift in

the absorption spectrum could be associated with In doping. As there is no significant difference in the electrical properties of all samples, it could be concluded that sample 15 (311)B is the best among all other samples investigated in this work because its absorption energy has the largest red-shift meaning that it is a more suitable material for solar cells with enhanced efficiency. Finally, a very interesting result, not reported in the literature, is that the GaAs (311)B orientation influences two properties that are important in semiconductor devices: (a) the crystalline quality of TiO_2 films improves as the thickness of the indium film used in doping increases; (b) the doping process is enhanced due to an increase of the incorporation of indium atoms.

Acknowledgements

F. S. A would like to thank Qassim University, Saudi Arabia, for funding his PhD studies. Y. G. G acknowledges Fundação de Amparo a Pesquisa do Estado de São Paulo (grants: 16/10668-7 and 18/01808-5). D. de Souza acknowledges the PhD fellowship from the Coordenação de Aperfeiçoamento de Pessoal de Nível Superior (CAPES). J. F. F also acknowledges the financial support from the Brazilian agencies Cnpq (Grant number: 303866/2018-7) and FAPDF (Grant number:193.001.757/2017). A. M. A. and A. Y. A. gratefully acknowledge King Abdulaziz City for Science and Technology (KACST) for the financial support.

Data Availability

The raw/processed data required to reproduce these findings cannot be shared at this time as the data also forms part of an ongoing study.

References

1. Hashimoto, K., H. Irie, and A. Fujishima, *TiO2 photocatalysis: a historical overview and future prospects.* Japanese journal of applied physics, 2005. **44**(12R): p. 8269.
2. Sarkar, M.B., et al., *Enlarged broad band photodetection using Indium doped TiO2 alloy thin film.* Journal of Alloys and Compounds, 2014. **615**: p. 440-445.
3. Chinnamuthu, P., et al., *Band gap enhancement of glancing angle deposited TiO2 nanowire array.* Journal of Applied Physics, 2012. **112**(5): p. 054315.
4. Henderson, M.A., *A surface science perspective on photocatalysis.* Surface Science Reports, 2011. **66**(6): p. 185-297.
5. Fujishima, A., X. Zhang, and D.A. Tryk, *TiO 2 photocatalysis and related surface phenomena.* Surface Science Reports, 2008. **63**(12): p. 515-582.
6. Fujishima, A. and K. Honda, *Electrochemical photolysis of water at a semiconductor electrode.* nature, 1972. **238**(5358): p. 37-38.
7. Xie, T., et al., *UV-assisted room-temperature chemiresistive NO 2 sensor based on TiO 2 thin film.* Journal of alloys and compounds, 2015. **653**: p. 255-259.
8. Liu, L., et al., *Room temperature impedance spectroscopy-based sensing of formaldehyde with porous TiO2 under UV illumination.* Sensors and Actuators B: Chemical, 2013. **185**: p. 1-9.
9. Cao, C., et al., *UV sensor based on TiO2 nanorod arrays on FTO thin film.* Sensors and Actuators B: Chemical, 2011. **156**(1): p. 114-119.
10. Diebold, U., *The surface science of titanium dioxide.* Surface science reports, 2003. **48**(5): p. 53-229.
11. Park, N.v., J. Van de Lagemaat, and A. Frank, *Comparison of dye-sensitized rutile-and anatase-based TiO2 solar cells*. 2000, National Renewable Energy Laboratory (NREL), Golden, CO.
12. Howard, C., T. Sabine, and F. Dickson, *Structural and thermal parameters for rutile and anatase.* Acta Crystallographica Section B: Structural Science, 1991. **47**(4): p. 462-468.
13. Reyes-Coronado, D., et al., *Phase-pure TiO2 nanoparticles: anatase, brookite and rutile.* Nanotechnology, 2008. **19**(14): p. 145605.
14. Amtout, A. and R. Leonelli, *Optical properties of rutile near its fundamental band gap.* Physical Review B, 1995. **51**(11): p. 6842.
15. Tang, H., et al., *Urbach tail of anatase TiO 2.* Physical Review B, 1995. **52**(11): p. 7771.
16. Wang, E., W. Yang, and Y. Cao, *Unique surface chemical species on indium doped TiO2 and their effect on the visible light photocatalytic activity.* The Journal of Physical Chemistry C, 2009. **113**(49): p. 20912-20917.
17. Gupta, K., et al., *Photocatalytic antibacterial performance of TiO2 and Ag-doped TiO2 against S. aureus. P. aeruginosa and E. coli.* Beilstein journal of nanotechnology, 2013. **4**(1): p. 345-351.
18. Bechstein, R., et al., *The effects of antimony doping on the surface structure of rutile TiO2 (110).* Nanotechnology, 2009. **20**(26): p. 264003.
19. Choi, W., A. Termin, and M.R. Hoffmann, *The role of metal ion dopants in quantum-sized TiO2: correlation between photoreactivity and charge*

carrier recombination dynamics. The Journal of Physical Chemistry, 1994. **98**(51): p. 13669-13679.

20. Al Saqri, N.A., et al., *Investigation of defects in indium doped TiO 2 thin films using electrical and optical techniques.* Journal of Alloys and Compounds, 2017. **698**: p. 883-891.
21. Al mashary, F.S., et al., *Effect of growth techniques on the structural, optical and electrical properties of indium doped TiO2 thin films.* Journal of Alloys and Compounds, 2018. **766**: p. 194-203.
22. Blakemore, J., *Semiconducting and other major properties of gallium arsenide.* Journal of Applied Physics, 1982. **53**(10): p. R123-R181.
23. Lee, M.-K., C.-F. Yen, and J.-J. Huang, *Electrical Characteristics of Liquid-Phase-Deposited TiO2 Films on GaAs Substrate with (NH4) 2S x Treatment.* Journal of The Electrochemical Society, 2006. **153**(5): p. F77-F80.
24. Şafak-Asar, Y., et al., *Investigation of dielectric relaxation and ac electrical conductivity using impedance spectroscopy method in (AuZn)/TiO2/p-GaAs (1 1 0) schottky barrier diodes.* Journal of Alloys and Compounds, 2015. **628**: p. 442-449.
25. Jameel, D., et al., *Electrical performance of conducting polymer (SPAN) grown on GaAs with different substrate orientations.* Applied Surface Science, 2016. **387**: p. 228-236.
26. Polimeni, A., et al., *Optical properties and device applications of (InGa) As self-assembled quantum dots grown on (311) B GaAs substrates.* Applied physics letters, 1998. **73**(10): p. 1415-1417.
27. Wang, L., et al., *Effect of interfacial bonds on the morphology of InAs QDs grown on GaAs (311) B and (100) substrates.* Nanoscale research letters, 2009. **4**(7): p. 689.
28. Dutta, S., R. Pal, and R. Chatterjee, *Electrical properties of spin coated ultrathin titanium oxide films on GaAs.* Materials Research Express, 2015. **2**(4): p. 046404.
29. Yen, C.-F. and M.-K. Lee, *Low equivalent oxide thickness of TiO2/GaAs MOS capacitor.* Solid-State Electronics, 2012. **73**: p. 56-59.
30. Qiu, J., et al., *Microscopic study of atomic layer deposition of TiO2 on GaAs and its photocatalytic application.* Chemistry of Materials, 2015. **27**(23): p. 7977-7981.
31. Liu, X., et al., *Structural characterization of TiO2 thin films prepared by pulsed laser deposition on GaAs (1 0 0) substrates.* Applied surface science, 2001. **174**(1): p. 35-39.
32. Pemasiri, K., et al., *Quantum confinement of excitons in wurtzite InP nanowires.* Journal of Applied Physics, 2015. **117**(19): p. 194306.
33. Fickenscher, M., et al., *Optical, structural, and numerical investigations of GaAs/AlGaAs core–multishell nanowire quantum well tubes.* Nano letters, 2013. **13**(3): p. 1016-1022.
34. Nowotny, J., T. Bak, and M.A. Alim, *Dual mechanism of indium incorporation into TiO2 (Rutile).* The Journal of Physical Chemistry C, 2014. **119**(2): p. 1146-1154.
35. Morgan, B.J. and G.W. Watson, *Polaronic trapping of electrons and holes by native defects in anatase TiO 2.* Physical Review B, 2009. **80**(23): p. 233102.

36. Lang, D., *Deep-level transient spectroscopy: A new method to characterize traps in semiconductors.* Journal of applied physics, 1974. **45**(7): p. 3023-3032.
37. Sze, S.M. and M.K. Lee, *Semiconductor devices : physics and technology*. 2013, Singapore: Wiley.
38. Pillai, P., et al., *Extraction of Schottky barrier at the F-doped SnO2/TiO2 interface in Dye Sensitized solar cells.* Journal of Renewable and Sustainable Energy, 2014. **6**(1): p. 013142.
39. Werner, J.H., *Schottky barrier and pn-junctionI/V plots—Small signal evaluation.* Applied Physics A: Materials Science & Processing, 1988. **47**(3): p. 291-300.
40. Van, C.N. and K. Potje-Kamloth, *Electrical and NO x gas sensing properties of metallophthalocyanine-doped polypyrrole/silicon heterojunctions.* Thin Solid Films, 2001. **392**(1): p. 113-121.
41. Aydoğan, Ş., M. Sağlam, and A. Türüt, *On the barrier inhomogeneities of polyaniline/p-Si/Al structure at low temperature.* Applied surface science, 2005. **250**(1): p. 43-49.
42. Jameel, D., et al., *High-performance organic/inorganic hybrid heterojunction based on Gallium Arsenide (GaAs) substrates and a conjugated polymer.* Applied Surface Science, 2015. **357**: p. 2189-2197.
43. Korucu, D., et al., *Evaluation of lateral barrier height of inhomogeneous photolithography-fabricated Au/n-GaAs Schottky barrier diodes from 80 K to 320 K.* Materials Science in Semiconductor Processing, 2012. **15**(5): p. 480-485.
44. Chand, S. and J. Kumar, *Evidence for the double distribution of barrier heights in Schottky diodes from I-V-T measurements.* Semiconductor science and technology, 1996. **11**(8): p. 1203.
45. Aziz, M., et al., *Electrical Behavior of MBE Grown Interfacial Misfit GaSb/GaAs Heterostructures With and Without Te-Doped Interfaces.* IEEE Transactions on Electron Devices, 2015. **62**(12): p. 3980-3986.
46. Tripathi, S. and M. Sharma, *Analysis of the forward and reverse bias IV and CV characteristics on Al/PVA: n-PbSe polymer nanocomposites Schottky diode.* Journal of Applied Physics, 2012. **111**(7): p. 074513.
47. Miyagi, T., et al., *Photocatalytic property and deep levels of Nb-doped anatase TiO2 film grown by metalorganic chemical vapor depostion.* Japanese journal of applied physics, 2004. **43**(2R): p. 775.
48. Pallotti, D.K., et al., *Photoluminescence Mechanisms in Anatase and Rutile TiO2.* The Journal of Physical Chemistry C, 2017. **121**(16): p. 9011-9021.
49. Gallart, M., et al., *Temperature dependent photoluminescence of anatase and rutile TiO2 single crystals: Polaron and self-trapped exciton formation.* Journal of Applied Physics, 2018. **124**(13): p. 133104.
50. Tang, H., et al., *Photoluminescence in TiO2 anatase single crystals.* Solid State Communications, 1993. **87**(9): p. 847-850.
51. Iijima, K., et al., *Influence of oxygen vacancies on optical properties of anatase TiO2 thin films.* Journal of Luminescence, 2008. **128**(5-6): p. 911-913.
52. Chan, C.-H., et al., *Optical characterization of structural quality in the formation of In2O3 thin-film nanostructures.* The Journal of Physical Chemistry C, 2016. **120**(38): p. 21983-21989.

53. Vurgaftman, I., J.á. Meyer, and L.á. Ram-Mohan, *Band parameters for III–V compound semiconductors and their alloys.* Journal of applied physics, 2001. **89**(11): p. 5815-5875.
54. Di Paola, A., M. Bellardita, and L. Palmisano, *Brookite, the least known TiO2 photocatalyst.* Catalysts, 2013. **3**(1): p. 36-73.
55. Shioi, K., et al., *Photoluminescence and thermal stability of yellow-emitting Sr-α-SiAlON: Eu2+ phosphor.* Journal of materials science, 2010. **45**(12): p. 3198-3203.
56. de Castro, S., et al., *Defects-related optical properties of Zn1− xCdxO thin films.* Materials Science and Engineering: B, 2016. **212**: p. 96-100.
57. Dobaczewski, L., A. Peaker, and K. Bonde Nielsen, *Laplace-transform deep-level spectroscopy: The technique and its applications to the study of point defects in semiconductors.* Journal of Applied Physics, 2004. **96**(9): p. 4689-4728.